A remarkable two-dimensional membrane for multifunctional gas separation: halogenated metal-free fused-ring polyphthalocyanine

Zhaoshun Meng,[ab] Yadong Zhang,[a] Qi Shi,[a] Yuzhen Liu,[a] Aijun Du*[b] and Ruifeng Lu*[a]

[a]Department of Applied Physics, Nanjing University of Science and Technology, Nanjing 210094, People's Republic of China
[b]School of Chemistry, Physics and Mechanical Engineering, Queensland University of Technology, Brisbane 4001, Australia

Section S1. Table S1: Force field (FF) parameters adopted in classical molecular dynamics (MD) simulations.

Section S2. Fig. S1–S6: First-principles MD simulation results at 300 and 500 K for pristine, F- and Cl-H_2PPc.

Section S3. The derivations of mechanical properties under infinitesimal strain theory and finite strain theory and Fig. S7: the second Piola–Kirchhoff (PK2) stress versus Lagrangian strain under uniaxial tension (*x*-direction) and under biaxial tension for pristine, F- and Cl-H_2PPc.

Section S4. Table S2: Adsorption energy for H_2, CO, CH_4, CO_2 and N_2 adsorbing on pore-II of pristine, F- and Cl-H_2PPc.

Section S5. Table S3–S5: Top view, side view and corresponding energy (eV) of the structures of the initial state (IS), the transition state (TS) and the final state (FS) for H_2, CO, CH_4, CO_2 and N_2 passing through pristine, F- and Cl-H_2PPc.

Section S6. Fig. S8–S9: Sketch of the minimum energy path for H_2, CO, CH_4, CO_2 and N_2 passing through F- and Cl-H_2PPc.

Section S7. Fig. S10: Pore areas of pore-I in F- and Cl-H_2PPc.

Section S1

Table S1 FF parameters of F-H_2PPc adopted in classical MD simulations.

	ε (kcal/mol)	σ (Å)
C	0.148	3.617
N	0.167	3.501
F	0.069	3.081
H	0.038	2.450

Section S2

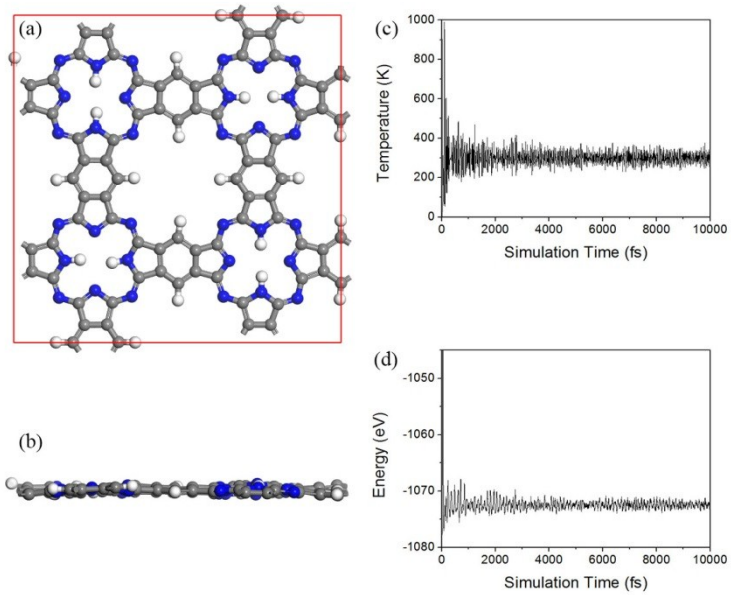

Fig. S1 (a) Top view and (b) side view of H_2PPc after 10 ps first-principles MD simulation at 300 K, and (c) temperature and (d) energy during the simulation. Grey, blue, and white balls stand for C, N, and H atoms.

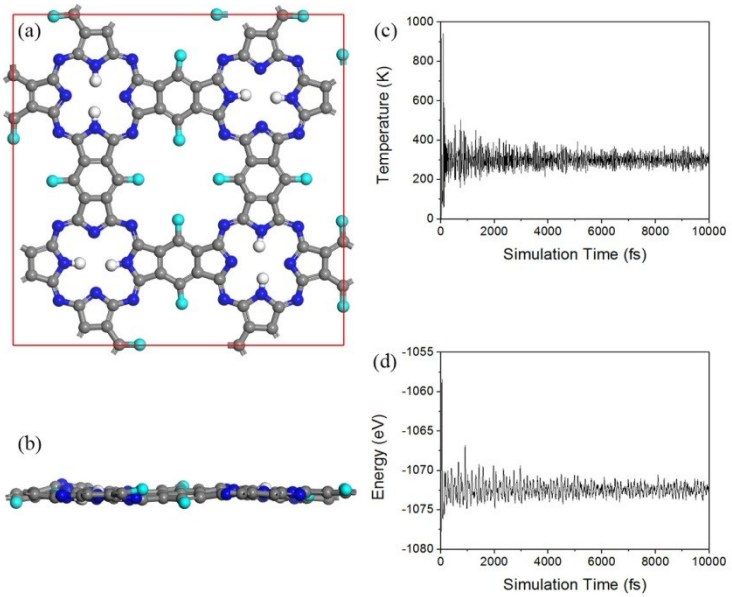

Fig. S2 (a) Top view and (b) side view of F-H_2PPc after 10 ps first-principles MD simulation at 300 K, and (c) temperature and (d) energy during the simulation. Grey, blue, white, and cyan balls stand for C, N, H, and F atoms.

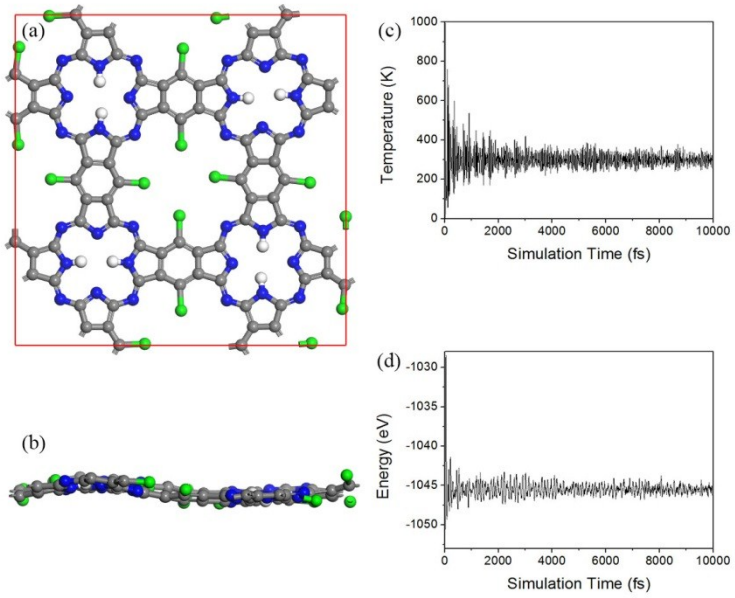

Fig. S3 (a) Top view and (b) side view of Cl-H_2PPc after 10 ps first-principles MD simulation at 300 K, and (c) temperature and (d) energy during the simulation. Grey, blue, white and green balls stand for C, N, H and Cl atoms.

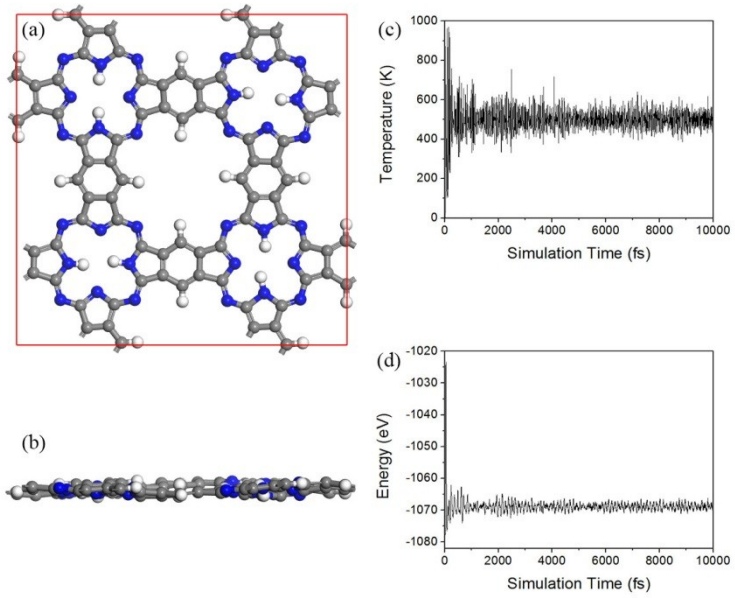

Fig. S4 (a) Top view and (b) side view of H_2PPc after 10 ps first-principles MD simulation at 500 K, and (c) temperature and (d) energy during the simulation. Grey, blue, and white balls stand for C, N, and H atoms.

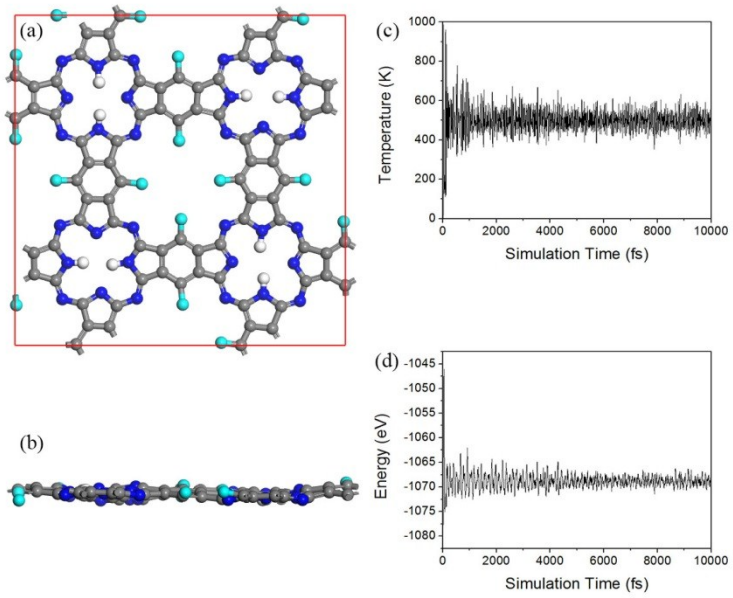

Fig. S5 (a) Top view and (b) side view of F-H_2PPc after 10 ps first-principles MD simulation at 500 K, and (c) temperature and (d) energy during the simulation. Grey, blue, white, and cyan balls stand for C, N, H, and F atoms.

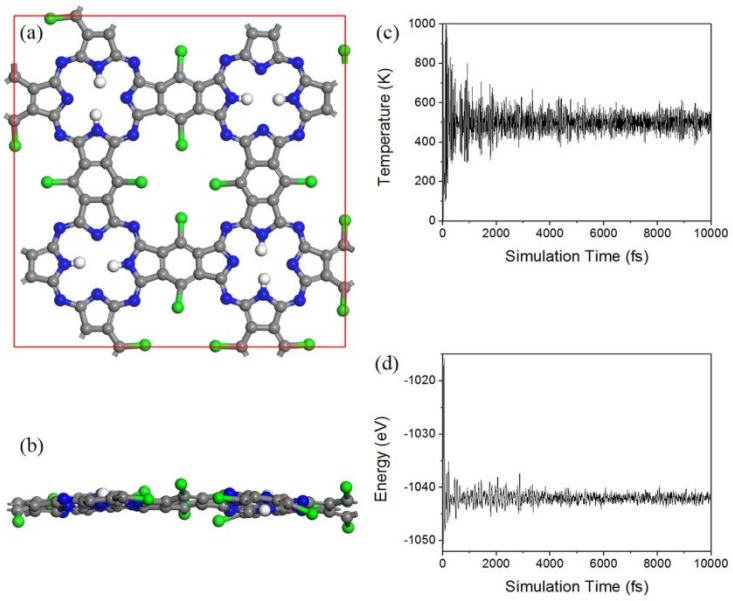

Fig. S6 (a) Top view and (b) side view of Cl-H_2PPc after 10 ps first-principles MD simulation at 500 K, and (c) temperature and (d) energy during the simulation. Grey, blue, white and green balls stand for C, N, H and Cl atoms.

Section S3

The involved structures all belong to the tetragonal crystal family of which only one in-plane Young's modulus as well as one Poisson's ratio along the *x*-direction (equivalent to *y*-direction) needs to be determined. In addition, the strength of studied membranes under uniaxial and biaxial tension is another important mechanical property that we expect to know.

1. The in-plane Young's modulus and Poisson's ratio under infinitesimal strain theory

For the in-plane Young's modulus (Y) and Poisson's ratio (μ) calculations, we adopted the linear approximation of stress–strain relationship under infinitesimal strain of 0–0.05.[1,2] As a result, the Hooke's law in three-dimensional materials is

$$\begin{pmatrix}\sigma_1\\ \sigma_2\\ \sigma_3\\ \sigma_4\\ \sigma_5\\ \sigma_6\end{pmatrix}=\begin{pmatrix}C_{11} & C_{12} & C_{13} & C_{14} & C_{15} & C_{16}\\ C_{12} & C_{22} & C_{23} & C_{24} & C_{25} & C_{26}\\ C_{13} & C_{23} & C_{33} & C_{34} & C_{35} & C_{36}\\ C_{14} & C_{24} & C_{34} & C_{44} & C_{45} & C_{46}\\ C_{15} & C_{25} & C_{35} & C_{45} & C_{55} & C_{56}\\ C_{16} & C_{26} & C_{36} & C_{46} & C_{56} & C_{66}\end{pmatrix}\begin{pmatrix}\varepsilon_1\\ \varepsilon_2\\ \varepsilon_3\\ \varepsilon_4\\ \varepsilon_5\\ \varepsilon_6\end{pmatrix} \quad (1)$$

in which the column matrices of stress and strain with Voigt notation[3] represent the stress and strain tensor respectively:

$$\sigma=\begin{pmatrix}\sigma_1 & \sigma_6 & \sigma_5\\ \sigma_6 & \sigma_2 & \sigma_4\\ \sigma_5 & \sigma_4 & \sigma_3\end{pmatrix}=\begin{pmatrix}\sigma_{xx} & \sigma_{xy} & \sigma_{xz}\\ \sigma_{xy} & \sigma_{yy} & \sigma_{yz}\\ \sigma_{xz} & \sigma_{yz} & \sigma_{zz}\end{pmatrix} \quad (2)$$

$$\varepsilon=\begin{pmatrix}\varepsilon_1 & \frac{1}{2}\varepsilon_6 & \frac{1}{2}\varepsilon_5\\ \frac{1}{2}\varepsilon_6 & \varepsilon_2 & \frac{1}{2}\varepsilon_4\\ \frac{1}{2}\varepsilon_5 & \frac{1}{2}\varepsilon_4 & \varepsilon_3\end{pmatrix}=\begin{pmatrix}\varepsilon_{xx} & \frac{1}{2}\gamma_{xy} & \frac{1}{2}\gamma_{xz}\\ \frac{1}{2}\gamma_{xy} & \varepsilon_{yy} & \frac{1}{2}\gamma_{yz}\\ \frac{1}{2}\gamma_{xz} & \frac{1}{2}\gamma_{yz} & \varepsilon_{zz}\end{pmatrix} \quad (3)$$

where σ_{ij} indicates that stress with *j*-direction orientation acts on the plane with an external normal direction of *i*, ε_{ii} means normal strain along the axis of *i* and γ_{ij} stands for shear strain between axes of *i* and *j*. The C_{ij} matrix represents the elastic stiffness constant with twenty-one independent elements at most.[3] The tetragonal crystal system with symmetry of D_{4h} possesses six independent matrix elements as:[3]

$$\begin{pmatrix}C_{11} & C_{12} & C_{13} & 0 & 0 & 0\\ & C_{11} & C_{13} & 0 & 0 & 0\\ & & C_{33} & 0 & 0 & 0\\ & & & C_{44} & 0 & 0\\ & & & & C_{44} & 0\\ & & & & & C_{66}\end{pmatrix} \quad (4)$$

so we get a simple form by applying 3D Hooke's law in two-dimensional studied monolayers:

$$\begin{cases}\sigma_1 = C_{11}\varepsilon_1 + C_{12}\varepsilon_2 \\ \sigma_2 = C_{12}\varepsilon_1 + C_{11}\varepsilon_2\end{cases} \tag{5}$$

According to the superposition principle under infinitesimal strain approximation:

$$\begin{cases}\varepsilon_1 = \frac{1}{Y}(\sigma_1 - \mu\sigma_2) \\ \varepsilon_2 = \frac{1}{Y}(\sigma_2 - \mu\sigma_1)\end{cases} \tag{6}$$

from which we derived:

$$\begin{cases}\sigma_1 = \frac{Y}{1-\mu^2}(\varepsilon_1 + \mu\varepsilon_2) \\ \sigma_2 = \frac{Y}{1-\mu^2}(\mu\varepsilon_1 + \varepsilon_2)\end{cases} \tag{7}$$

So we easily obtained the in-plane Young's modulus and the Poisson's ratio as:

$$\begin{cases}Y = C_{11} - \frac{C_{12}^2}{C_{11}} \\ \mu = \frac{C_{12}}{C_{11}}\end{cases} \tag{8}$$

Thus, two matrix elements of C_{11} and C_{12} should be known to calculate Y and μ. The density of structures' total energy difference can be expressed as Taylor series expansion under the infinitesimal strain approximation:

$$\frac{\Delta E}{V} = \frac{1}{2}C_{11}\varepsilon_1^2 + \frac{1}{2}C_{11}\varepsilon_2^2 + C_{12}\varepsilon_1\varepsilon_2 \tag{9}$$

That is to say, let ε_1 and ε_2 vary from 0 to 0.03 by an increment of 0.005, we could get the value of C_{11} and C_{12} by fitting data of the density of total energy difference versus strain. Note that, the transformation of lattice vectors from R to R' is computed by $R_i^{'} = FR_i = (\varepsilon + I)R_i$,[1,4,5] in which F is the deformation gradient tensor and I is the identity tensor. The fitted surfaces are drawn in Figure 1 in the main text.

2. The strength under finite strain theory

With respect to the strength of studied structures, i.e. the ultimate strain and the ultimate stress, the finite strain theory is employed instead of the infinitesimal strain approximation. The finite strain brings more specific definition of strain and stress and the curves of the second Piola–Kirchhoff (PK2) stress versus the Lagrangian strain are needed to observe the strength of materials. The Lagrangian strain is defined as:

$$\eta = \frac{1}{2}(F^T F - I) \tag{10}$$

For uniaxial tensions, the Lagrangian strain tensor and the deformation gradient tensor are respectively

$$\eta_{uniaxial} = \begin{pmatrix} \delta & 0 & 0 \\ 0 & 0 & 0 \\ 0 & 0 & 0 \end{pmatrix} \tag{11}$$

and

$$F_{uniaxial} = \begin{pmatrix} \varepsilon + 1 & 0 & 0 \\ 0 & 1 & 0 \\ 0 & 0 & 1 \end{pmatrix} \tag{12}$$

Therefore, in a range of 0–0.3 with an increment of 0.02 for the Lagrangian strain element δ, we can obtain transformed structures by the transformation gradient tensor and compute their stresses by further. Note that the associated deformation gradient tensor is not unique for a given Lagrangian strain tensor, however only differing by a rigid rotation from one to another. Since the rigid deformation does not change the relative position of the atoms and the desired stress and energy,[6,7] we take the most uncomplicated treatment of the deformation gradient tensor by ignoring the rigid motion without losing any useful information. For biaxial tensions, the Lagrangian strain tensor and the deformation gradient tensor are respectively:

$$\eta_{biaxial} = \begin{pmatrix} \delta & 0 & 0 \\ 0 & \delta & 0 \\ 0 & 0 & 0 \end{pmatrix} \tag{13}$$

and

$$F_{biaxial} = \begin{pmatrix} \varepsilon + 1 & 0 & 0 \\ 0 & \varepsilon + 1 & 0 \\ 0 & 0 & 1 \end{pmatrix} \tag{14}$$

with the same data spacing for the Lagrangian strain element δ.

The stress calculated by the Vienna ab initio simulation package[8] is the true or Cauchy stress, σ, which related to PK2 stress as:

$$\Sigma = det(F)F^{-1}\sigma F^{-T} \tag{15}$$

Because the uniaxial and biaxial tensions lead to two nonzero elements of the true stress tensor, the σ can be written as:

$$\sigma = \begin{pmatrix} \sigma_1 & 0 & 0 \\ 0 & \sigma_2 & 0 \\ 0 & 0 & 0 \end{pmatrix} \tag{16}$$

Combined these equations, we deduce the PK2 stresses under uniaxial and biaxial tension are:

$$\Sigma_{uniaxial} = \begin{pmatrix} \dfrac{\sigma_1}{(\varepsilon + 1)} & 0 & 0 \\ 0 & (\varepsilon + 1)\sigma_2 & 0 \\ 0 & 0 & 0 \end{pmatrix} \tag{17}$$

$$\Sigma_{biaxial} = \begin{pmatrix} \sigma_1 & 0 & 0 \\ 0 & \sigma_2 & 0 \\ 0 & 0 & 0 \end{pmatrix} \tag{18}$$

The curves of two components of PK2 stress versus Lagrangian strain are drawn in Fig. S7.

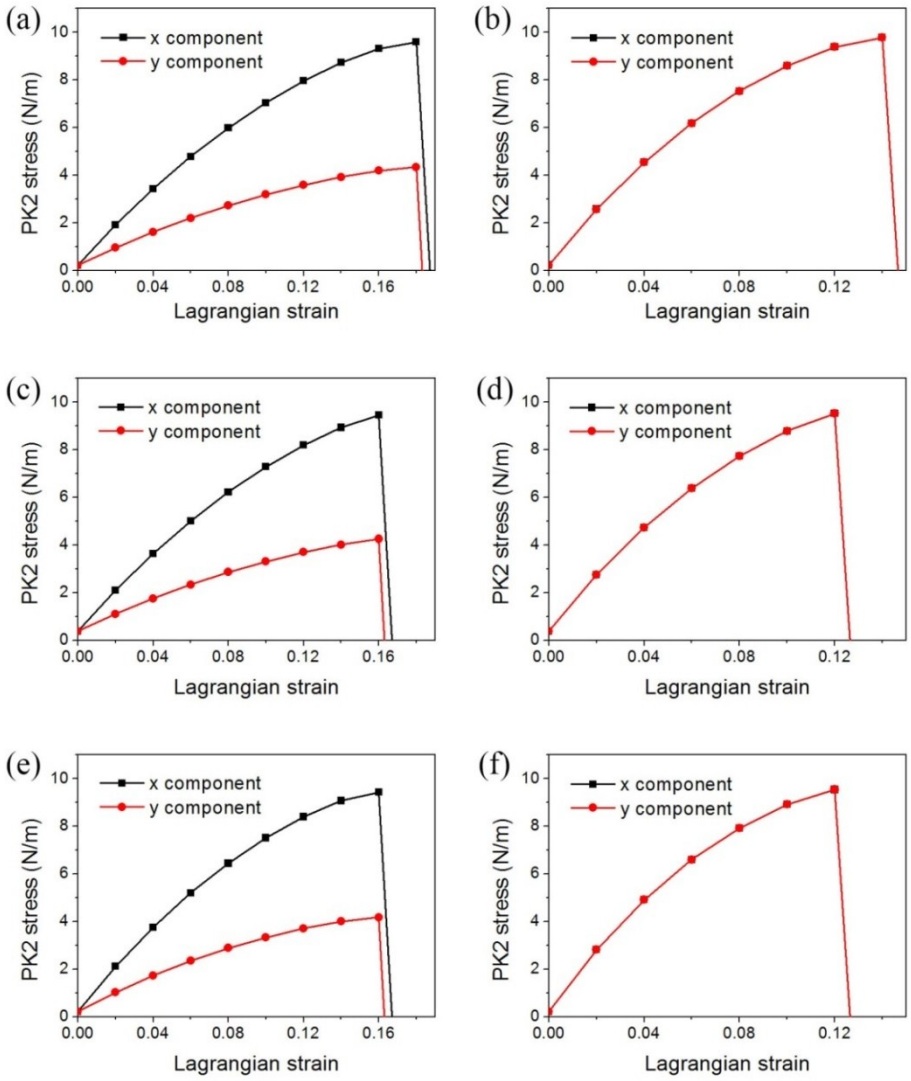

Fig. S7 PK2 stress versus Lagrangian strain under uniaxial tension (*x*-direction) for (a) H_2PPc, (c) F-H_2PPc and (e) Cl-H_2PPc and under biaxial tension for (b) H_2PPc, (d) F-H_2PPc and (f) Cl-H_2PPc.

Section S4

Table S2 Adsorption energy (eV) for H_2, CO, CH_4, CO_2 and N_2 adsorbing on pore-II of pristine, F- and Cl-H_2PPc.

	H_2	CO	CH_4	CO_2	N_2
H_2PPc	0.07	0.13	0.13	0.18	0.12
F-H_2PPc	0.07	0.13	0.13	0.18	0.12
Cl-H_2PPc	0.13	0.22	0.23	0.25	0.18

Section S5

Table S3 Top view, side view and corresponding energy (eV) of the structures of IS, TS and FS for H_2, CO, CH_4, CO_2 and N_2 passing through pristine H_2PPc.

Gas	Property	Initial State	Transition State	Final State
H_2	Top View	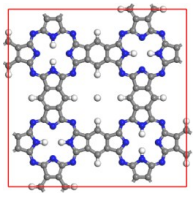	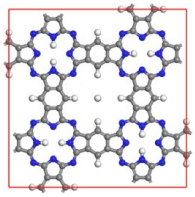	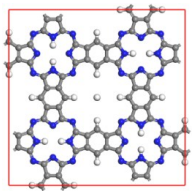
	Side View	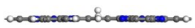		
	Energy	–1085.09	–1085.09	–1085.09
CO	Top View	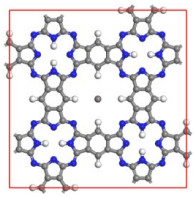	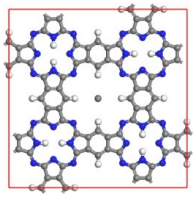	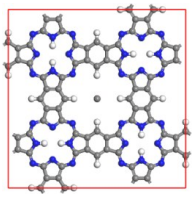
	Side View	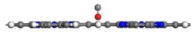	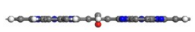	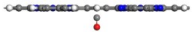
	Energy	–1093.16	–1093.14	–1093.17
CH_4	Top View	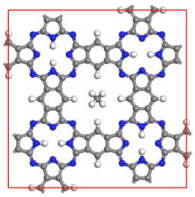	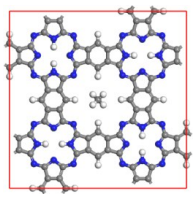	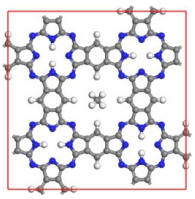
	Side View	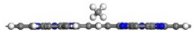		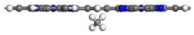
	Energy	–1102.44	–1102.45	–1102.44
CO_2	Top View	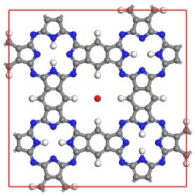	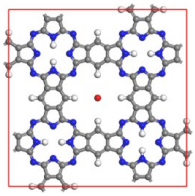	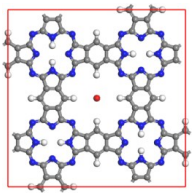
	Side View	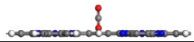	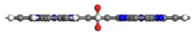	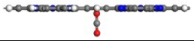
	Energy	–1101.38	–1101.36	–1101.38
N_2	Top View	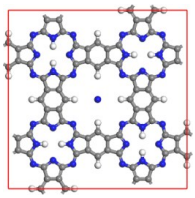	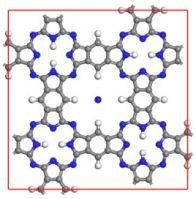	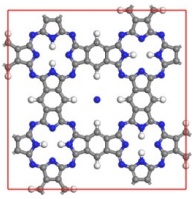
	Side View	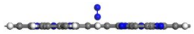	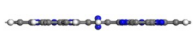	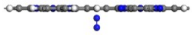
	Energy	–1095.00	–1094.98	–1095.00

Table S4 Top view, side view and corresponding energy (eV) of the structures of IS, TS and FS for H_2, CO, CH_4, CO_2 and N_2 passing through F-H_2PPc.

Gas	Property	Initial State	Transition State	Final State
H_2	Top View	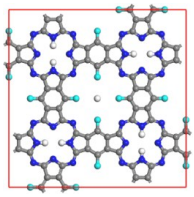	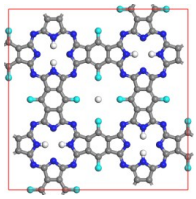	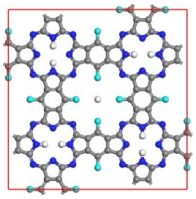
	Side View	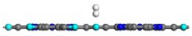		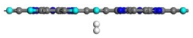
	Energy	–1085.16	–1085.10	–1085.16
CO	Top View	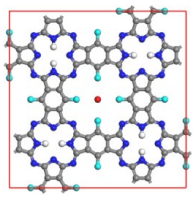	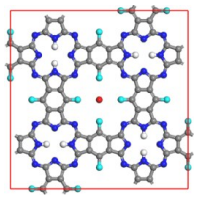	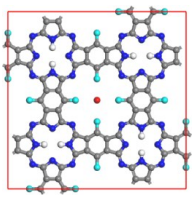
	Side View	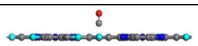	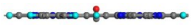	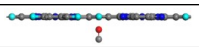
	Energy	–1093.19	–1092.99	–1093.20
CH_4	Top View	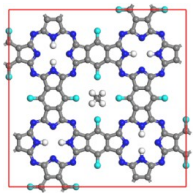	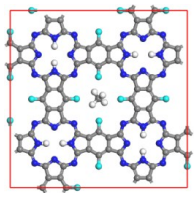	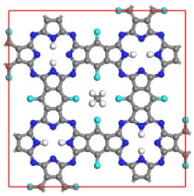
	Side View	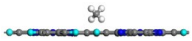		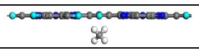
	Energy	–1102.50	–1101.88	–1102.50
CO_2	Top View	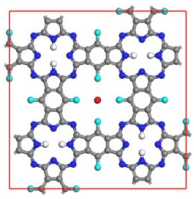	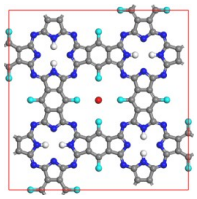	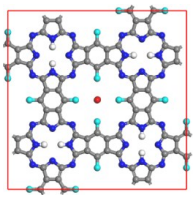
	Side View	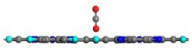	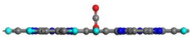	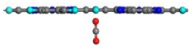
	Energy	–1101.36	–1101.31	–1101.36
N_2	Top View	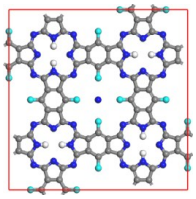	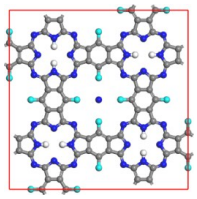	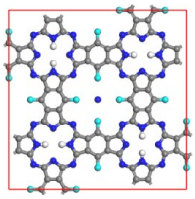
	Side View	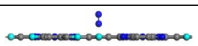	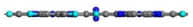	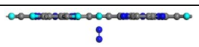
	Energy	–1095.05	–1094.81	–1095.05

Table S5 Top view, side view and corresponding energy (eV) of the structures of IS, TS and FS for H_2, CO, CH_4, CO_2 and N_2 passing through Cl-H_2PPc.

Gas	Property	Initial State	Transition State	Final State
H_2	Top View	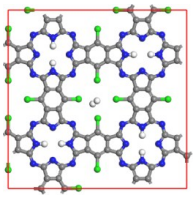	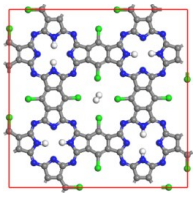	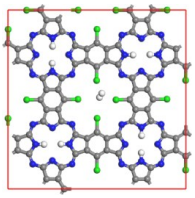
	Side View	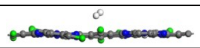	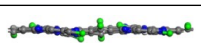	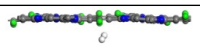
	Energy	–1058.12	–1057.57	–1058.13
CO	Top View	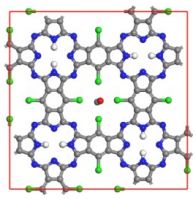	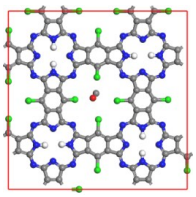	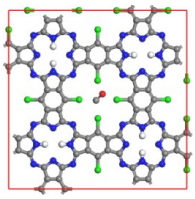
	Side View	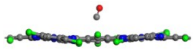	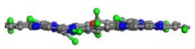	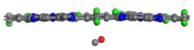
	Energy	–1066.18	–1065.14	–1066.19
CH_4	Top View	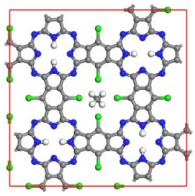	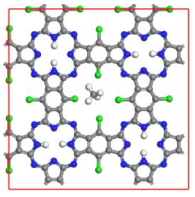	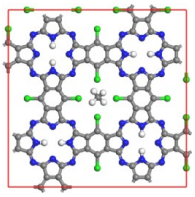
	Side View	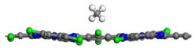	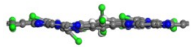	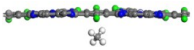
	Energy	–1075.46	–1074.09	–1075.46
CO_2	Top View	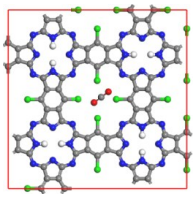	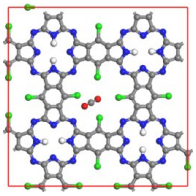	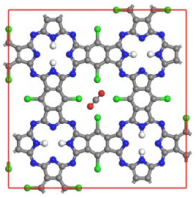
	Side View	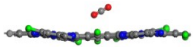	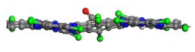	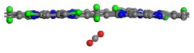
	Energy	–1074.42	–1072.92	–1074.40
N_2	Top View	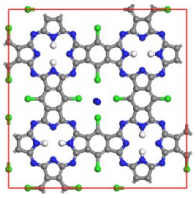	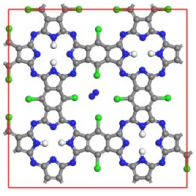	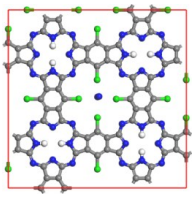
	Side View	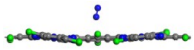	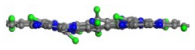	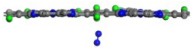
	Energy	–1068.02	–1066.92	–1068.01

Section S6

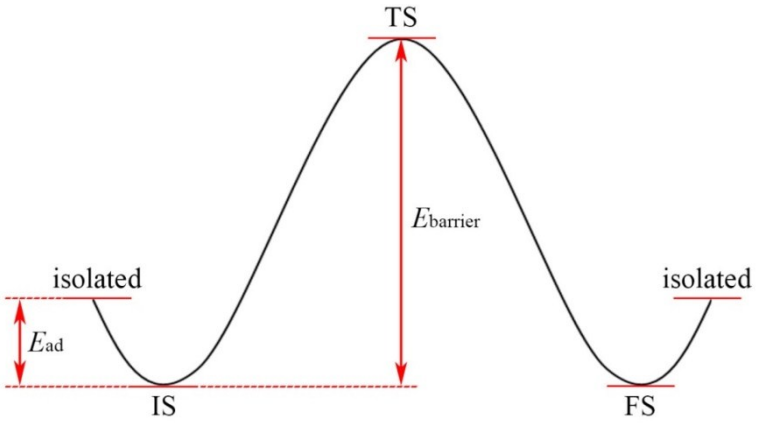

Fig. S8 Sketch of the minimum energy path for H_2, CO, CH_4 and N_2 passing through F- and Cl-H_2PPc.

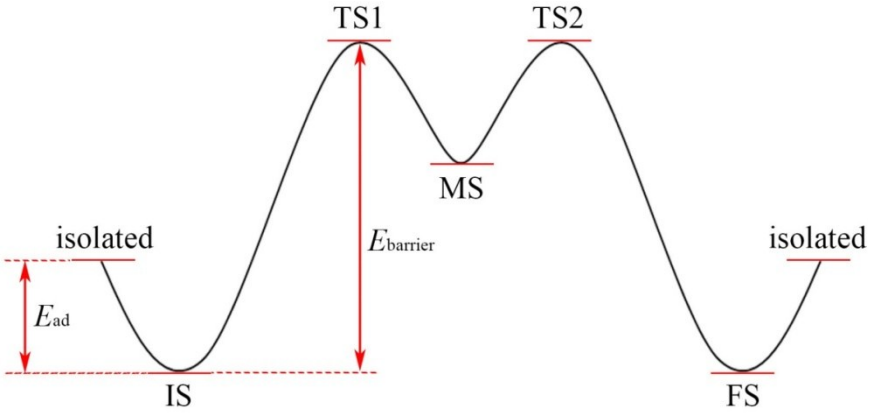

Fig. S9 Sketch of the minimum energy path for CO_2 passing through F- and Cl-H_2PPc.

Section S7

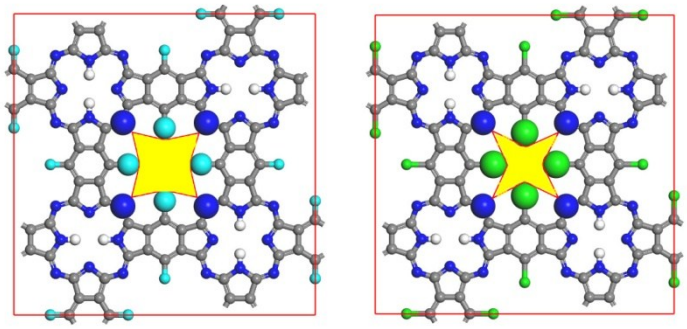

Fig. S10 Yellow areas stand for the pore areas in F- and Cl-H_2PPc. Grey, blue, white, cyan and green balls stand for C, N, H, F and Cl atoms. Larger balls represent atoms with R_{eff} at pore-I.

References

1 X. Wei, B. Fragneaud, C. A. Marianetti and J. W. Kysar, *Phys. Rev. B*, 2009, **80**, 205407.

2 Y. Y. Zhang, Q. X. Pei and C. M. Wang, *Appl. Phys. Lett.*, 2012, **101**, 081909.

3 J. F. Nye, *Physical Properties of Crystals: Their Representation by Tensors and Matrices.* Clarendon Press, 1985.

4 Q. Peng, W. Ji and S. De, *Phys. Chem. Chem. Phys.*, 2012, **14**, 13385–13391.

5 Q. Peng, W. Ji and S. De, *Comp. Mater. Sci.*, 2012, **56**, 11–17.

6 J. Zhao, J. M. Winey and Y. M. Gupta, *Phys. Rev. B*, 2007, **75**, 094105.

7 J. Zhou and R. Huang, *J. Mech. Phys. Solids*, 2008, **56**, 1609–1623.

8 G. Kresse and J. Furthmüller, *Phys. Rev. B*, 1996, **54**, 11169–11186.